Geophysical Journal International

Geophys. J. Int. (2017) **208,** 468–481
Advance Access publication 2016 October 20
GJI Seismology

doi: 10.1093/gji/ggw395

Spatiotemporal variations of interplate slip rates in northeast Japan inverted from recurrence intervals of repeating earthquakes

Shunichi Nomura,[1] Yosihiko Ogata,[2,3] Naoki Uchida[4] and Mitsuhiro Matsu'ura[2]

[1] *Department of Mathematical and Computing Sciences, Tokyo Institute of Technology, Tokyo, Japan. E-mail: nomura@is.titech.ac.jp*
[2] *The Institute of Statistical Mathematics, Tokyo, Japan*
[3] *Earthquake Research Institute, the University of Tokyo, Tokyo, Japan*
[4] *Graduate School of Science, Tohoku University, Sendai, Japan*

Accepted 2016 October 18. Received 2016 October 13; in original form 2016 June 1

SUMMARY

Repeating earthquakes, the sequence of stress accumulation and release at isolated small asperities on a plate interface, can be regarded as a renewal process in statistics. From such a point of view, we modelled a sequence of repeating earthquakes and developed an objective Bayesian method to estimate the space–time distribution of interplate slip rates from the recurrence intervals of repeating earthquakes. The space–time distribution of slip rates is represented by the superposition of tri-cubic B-splines. The knots of B-splines in time are unequally allocated for representing co-seismic abrupt and post-seismic rapid changes in slip rates. In addition, to avoid overfitting, smoothness constraints are imposed and their optimal weights are determined by Akaike's Bayesian Information Criterion. We applied this method to the complete data set of repeating earthquakes in northeast Japan for about 18 yr before the 2011 Tohoku-oki earthquake, and revealed spatiotemporal variations of interplate slip rates off the Hokkaido-Tohoku region, where the 1994 Sanriku-oki (M7.6), 2003 Tokachi-oki (M8.0), 2004 Kushiro-oki (M7.1), and 2008 Ibaraki-oki (M7.0) earthquakes occurred. First, we confirmed the reciprocal correlation between the spatial distribution of average slip rates for a seismically calm period (1996–2000) and that of average slip-deficit rates, which has been estimated from GPS array data. Then, we examined the temporal variations of slip rates associated with the large interplate earthquakes in detail.

Key words: Inverse theory; Spatial analysis; Seismic cycle; Seismicity and tectonics; Statistical seismology; Subduction zone processes.

1 INTRODUCTION

Nadeau *et al*. (1995) revealed the clustering and periodic recurrence of microearthquakes along the Parkfield segment of the San Andreas fault, California. Nadeau & Johnson (1998) showed that small earthquakes within these clusters have simple scaling relations for the seismic parameters of source area, fault slip, and recurrence interval, which indicate a sequence of repeating earthquakes to be a cyclic process of stress accumulation and release at an isolated small asperity on the plate interface. Based on the scaling relations for seismic parameters, Nadeau & McEvilly (1999) provided a simple method to estimate average fault slip rates at microearthquake clustering areas from the recurrence intervals of repeating earthquake sequences.

Igarashi *et al*. (2003) and Uchida *et al*. (2004) applied the basic idea and method proposed by Nadeau & Johnson (1998) and Nadeau & McEvilly (1999) to repeating earthquake sequences in northeast Japan, where the Pacific plate is descending beneath the North American plate, and estimated aseismic slip rates around the source regions of past and potential large interplate earthquakes. Using the complete data set of repeating earthquakes for 1993–2005, Uchida *et al*. (2009) examined the spatiotemporal variations of interplate aseismic slip rates associated with the 2003 Tokachi-oki earthquake (M8.0) and the 2004 Kushiro-oki earthquake (M7.1). After the occurrence of the 2011 Tohoku-oki earthquake (M9.0), using the complete data set for 1993–2007, Uchida & Matsuzawa (2011) estimated the spatial distribution of interplate coupling coefficients in and around the source region of the megathrust event. Then, using the complete data set for 1993–2011, Uchida & Matsuzawa (2013) examined the spatiotemporal variations of interplate aseismic slip rates associated with the 2011 Tohoku-oki earthquake in detail.

The distribution of repeating earthquakes is heterogeneous both in space and time. In the previous studies, because of the use of simple least-squares methods, the estimation of slip rates has been limited to specific space–time domains where a sufficiently large number of repeating earthquakes were observed. Recently, Nomura *et al*. (2014) proposed a statistical method to estimate the spatiotemporal change in stress loading rates from the recurrence intervals of repeating earthquakes. This method is based on a stochastic model of repeating earthquakes with the assumption of stress accumulation-release cycles at small asperities under Brownian perturbation (Matthews *et al.* 2002). An advantage of the stochastic modelling is that we can use information of quiescence before the first event and that after the last event of a sequence as well as occurrence times of repeating earthquakes on the theory of point processes.

In this paper, first, we modify the stochastic model proposed by Nomura *et al.* (2014) and develop a Bayesian statistical method to estimate the space–time distribution of interplate slip rates from the recurrence intervals of repeating earthquakes. Then, applying it to the complete data set of repeating earthquakes in northeast Japan for 1993–2011 (about 18 yr before the 2011 Tohoku-oki earthquake), we reveal spatiotemporal variations of interplate slip rates off the Hokkaido-Tohoku region in detail, where the 1994 Sanriku-oki (M7.6), 2003 Tokachi-oki (M8.0), 2004 Kushiro-oki (M7.1), and 2008 Ibaraki-oki (M7.0) earthquakes occurred. In addition, to examine the validity of our method, we compare the slip-rate distribution estimated from repeating earthquake data with the slip-deficit-rate distribution estimated from GPS array data for a specific period.

2 A STATISTICAL METHOD TO ESTIMATE INTERPLATE SLIP RATES

2.1 Fundamental relation between recurrence intervals and seismic moments

The occurrence of interplate earthquakes is the sudden release of shear stress accumulated at strength asperities on a plate interface (e.g. Lay & Kanamori 1981; Fukuyama *et al.* 2002; Hashimoto & Matsu'ura 2002; Hashimoto *et al.* 2014). A sequence of repeating earthquakes is considered to be a cyclic process of stress accumulation and release at an isolated small asperity, driven by relative plate motion. In the case of an isolated asperity with the effective area of A, the stress accumulation rate $\dot{\tau}$ is proportional to the background aseismic slip rate v and inversely proportional to the characteristic dimension $A^{1/2}$ of the asperity (e.g. Hashimoto & Matsu'ura 2000); that is,

$$\dot{\tau} = c\mu v A^{-1/2}, \tag{1}$$

where c is a geometrical factor and μ is the shear modulus. So, denoting the average stress drop by $\Delta\tau$, the recurrence interval T of repeating earthquakes is given by

$$T = \Delta\tau/\dot{\tau} = (c\mu)^{-1}\Delta\tau A^{1/2}/v. \tag{2}$$

Since the product of the background slip rate and the recurrence interval gives the average fault slip $d(= vT)$ of repeating earthquakes, the seismic moment M_0 is written as

$$M_0 = \mu d A = c^{-1}\Delta\tau A^{3/2}. \tag{3}$$

From eqs (2) and (3), we obtain a fundamental relation between the recurrence interval and the seismic moment as

$$T = c^{-2/3}(\mu v)^{-1}(M_0\Delta\tau^2)^{1/3}. \tag{4}$$

The above equation can be written as

$$\log T = -\log v + \tfrac{1}{3}\log M_0 + \text{const}, \tag{5}$$

if the stress drop is scale-independent, or

$$\log T = -\log v + \tfrac{1}{6}\log M_0 + \text{const}, \tag{6}$$

if the stress drop has the scale dependence of $\Delta\tau = c' M_0^{-1/4}$ as Nadeau & Johnson (1998) stated. In this study, we adopt the latter and use the following relation:

$$\log T = -\log v + \tfrac{1}{6}\log M_0 - 2.36, \tag{7}$$

which is equivalent to the empirical result of regression, $\log d = -2.36 + 0.17\log M_0$, obtained by Nadeau & Johnson (1998). Here, the recurrence intervals T and the seismic moments M_0 (or magnitude M) of repeating earthquakes are observable, and so we can set an inverse problem of estimating the space–time distribution of background slip rates v from various sequences of repeating earthquakes.

2.2 A non-stationary renewal model of repeating earthquakes

In this section, we give an outline of the non-stationary renewal model of repeating earthquakes proposed by Nomura *et al.* (2014) with some modifications to evaluate slip rates based on the ideas in the previous section. For mathematical details including the derivation of its likelihood function for parameter estimation, refer to their original paper.

We first define a stochastic model for a single sequence of repeating earthquakes for a specific period $[t_s, t_e]$. The sequence consists of n repeating earthquakes with their occurrence times $\{t_i; i = 1, \ldots, n\}$ and magnitudes $\{M_i; i = 1, \ldots, n\}$. Here, we use magnitude M, which can be transformed into seismic moment M_0 by the following formula (Kanamori 1977; Hanks & Kanamori 1979):

$$\log M_0 = \tfrac{3}{2}M + 16.1. \tag{8}$$

In general, the background slip rate v temporally fluctuates because of pre-seismic, co-seismic, and post-seismic slips of underlying large asperities, and so it should be represented as a function $v(t)$ of time. Then, the ith recurrence interval, $T_i \equiv t_{i+1} - t_i$, also fluctuates, because it depends on the background slip rate $v(t)$. The fluctuation of recurrence intervals is caused by not only the fluctuation of background aseismic slip rates but also external stress perturbation due to seismic and/or aseismic slip of adjacent large asperities. Matthews *et al.* (2002) modelled the recurrence intervals with latter-type fluctuation as the Brownian passage time (BPT) distribution. The BPT distribution for each recurrence interval has a mean recurrence interval T defined in eq. (7) and an aperiodicity parameter σ, which represents the strength of external stress perturbation. An advantage of the stochastic modelling is that we can use information of the quiescence before the first event, $t_1 - t_s$, and that after the last event, $t_e - t_n$, as well as occurrence times of repeating earthquakes on the theory of point processes (e.g. Daley & Vere-Jones 1988).

Following Matthews *et al.* (2002), we assume the BPT distribution of recurrence intervals T with its probability density function (PDF)

$$f(T \mid v, \sigma, d) = \frac{d}{\sqrt{2\pi\sigma^2 T^3}}\exp\left\{-\frac{(d - vT)^2}{2\sigma^2 T}\right\} \tag{9}$$

and the cumulative distribution function $F(T|v, \sigma, d) = \int_0^T f(T'|v, \sigma, d)\mathrm{d}T'$, where v and d correspond to the drift rate λ and the critical level x, respectively, in their description. Using eq. (8), we can rewrite Nadeau–Johnson's scaling relation as $\log d = \frac{1}{4}M + 0.377 + \varepsilon$. Here, we added a site-dependent correction term ε as an unknown parameter. Then, the likelihood function for a sequence of repeating earthquakes is given by

$$L_{[t_s,t_e]}(v,\sigma,\varepsilon\,|\,t_1,\ldots,t_n,M_1,\ldots,M_n)$$
$$=\frac{v}{\bar{d}}\left\{1-F(t_1-t_s\,|\,v,\sigma,\bar{d})\right\}\left\{\prod_{i=1}^{n-1}f(t_{i+1}-t_i\,|\,v,\sigma,d_i)\right\}$$
$$\times\left\{1-F(t_e-t_n\,|\,v,\sigma,d_n)\right\} \tag{10}$$

with $\bar{d}=(d_1+\ldots+d_n)/n$. Here, the first and last factors represent the likelihoods of the quiescence before the first event, t_1-t_s, and that after the last event, t_e-t_n, respectively.

As has been mentioned, the background slip rate v varies in time. Strictly speaking, we cannot directly apply the BPT distribution in eq. (9) to such a non-stationary case. So, we define a cumulative slip function as

$$s(t)=\int_{t_s}^{t}v(t')\mathrm{d}t', \tag{11}$$

and use it to measure the process of loading instead of actual time t (e.g. Lindqvist *et al.* 2003). With such time transformation, we can rewrite the fault slip vT_i of the ith event as $S_i=s(t_{i+1})-s(t_i)$ and exactly define its BPT distribution by the PDF $f(S|1,\sigma,d)$. Since $s(t)$ monotonously increases with time, we can apply the following transformation rule of PDF: $f(T|v,\sigma,d)=f(S|1,\sigma,d)(\mathrm{d}s/\mathrm{d}t)$. Then, the likelihood function for the non-stationary slip rate $v(t)$ is given by

$$L_{[t_s,t_e]}(v,\sigma,\varepsilon\,|\,t_1,\ldots,t_n,M_1,\ldots,M_n)$$
$$=L_{[0,s_e]}(1,\sigma,\varepsilon\,|\,s_1,\ldots,s_n,M_1,\ldots,M_n)\prod_{i=1}^{n}\left.\frac{\mathrm{d}s}{\mathrm{d}t}\right|_{t=t_i}$$
$$=\frac{v}{\bar{d}}\left\{1-F(s_1-0\,|\,1,\sigma,\bar{d})\right\}\left\{\prod_{i=1}^{n-1}f(s_{i+1}-s_i\,|\,1,\sigma,d_i)\right\}$$
$$\times\left\{1-F(s_e-s_n\,|\,1,\sigma,d_n)\right\}\prod_{i=1}^{n}v(t_i) \tag{12}$$

with $s_i=s(t_i)$ for $i=1,\ldots,n$ and $s_e=s(t_e)$.

Now, we extend the stochastic model for a single sequence in eq. (12) to the space–time model for multi-sequences of repeating earthquakes distributed on a plate interface. We consider m sequences of repeating earthquakes at various sites $\{x^{(j)},y^{(j)};j=1,\ldots,m\}$ on a plate interface. Hereafter, we use the superscript (j) to indicate anything for the jth site. Then, denoting $v^{(j)}(t)=v(x^{(j)},y^{(j)},t)$, we can write the combined likelihood function for all the m sequences as

$$L_{[t_s,t_e]}(v,\boldsymbol{\sigma},\boldsymbol{\varepsilon}\,|\,\mathbf{t},\mathbf{M})$$
$$=\prod_{j=1}^{m}L_{[t_s,t_e]}\left(v^{(j)},\sigma^{(j)},\varepsilon^{(j)}\,\middle|\,t_1^{(j)},\ldots,t_{n^{(j)}}^{(j)},M_1^{(j)},\ldots,M_{n^{(j)}}^{(j)}\right), \tag{13}$$

where v is a function of space and time, $\boldsymbol{\sigma}$ and $\boldsymbol{\varepsilon}$ are $m\times 1$ dimensional vectors, and $\mathbf{t}$ and $\mathbf{M}$ are $n\,(=\sum_{j=1}^{m}n^{(j)})\times 1$ dimensional vectors.

2.3 B-spline representation of space–time slip-rate distribution

We represent the slip-rate function $v(x,y,t)$ defined in a space–time domain $V=[x_s,x_e]\times[y_s,y_e]\times[t_s,t_e]$ by using cubic B-splines (e.g. de Boor 1978). We divide the space domain into $I\times J$ rectangular subsections by equally spaced knots, $\beta_i^x=x_s+i(x_e-x_s)/I$ for $i=0,1,\ldots,I$ and $\beta_j^y=y_s+j(y_e-y_s)/J$ for $j=0,1,\ldots,J$, and assign cubic B-splines, $B_{-1}^x,B_0^x,\ldots,B_{I+1}^x$ and $B_{-1}^y,B_0^y,\ldots,B_{J+1}^y$, to the extended knots, $\beta_{-1}^x,\beta_0^x,\ldots,\beta_{I+1}^x$ and $\beta_{-1}^y,\beta_0^y,\ldots,\beta_{J+1}^y$, respectively. For the time domain, we also assign cubic B-splines to knots in a similar way, but they are unequally allocated for representing co-seismic abrupt and post-seismic rapid changes in slip rates. When a large earthquake occurred in some region, for example, the time domain $[t_s,t_e]$ for that region should be divided into two parts, $[t_s,t_r]$ and $[t_r,t_e]$, at the occurrence time $t=t_r$ of the large earthquake. Hence, the number of partition K_{ij} for the time domain $[t_s,t_e]$ differs from region to region. We denote the cubic B-splines in time domain as $B_{ij,-1}^t,B_{ij,0}^t,\ldots,B_{ij,K_{ij}+1}^t$ for the ijth spatial domain. After all, we can define a 3-D B-spline function as

$$\psi(x,y,t;\boldsymbol{\alpha})=\sum_{i=-1}^{I+1}\sum_{j=-1}^{J+1}\sum_{k=-1}^{K_{ij}+1}\alpha_{ijk}B_i^x(x)B_j^y(y)B_{ij,k}^t(t), \tag{14}$$

where the set of coefficients $\boldsymbol{\alpha}=(\alpha_{ijk};i=-1,\ldots,I+1,j=-1,\ldots,J+1,k=-1,\ldots,K_{ij}+1)$ are unknown model parameters to be estimated. Then, to satisfy a postulate of irreversibility for interplate slip, we represent the slip-rate function $v(x,y,t)$ by the exponential of the B-spline function as

$$v(x,y,t;\boldsymbol{\alpha})=\exp\left\{\psi(x,y,t;\boldsymbol{\alpha})\right\}. \tag{15}$$

Substituting eq. (15) into eq. (13), we finally obtain the likelihood as a function of unknown parameters, $\boldsymbol{\alpha}$, $\boldsymbol{\sigma}$ and $\boldsymbol{\varepsilon}$:

$$L_{[t_s,t_e]}(\boldsymbol{\alpha},\boldsymbol{\sigma},\boldsymbol{\varepsilon}\,|\,\mathbf{t},\mathbf{M})$$
$$=\prod_{j=1}^{m}L_{[t_s,t_e]}\left(v^{(j)}(\cdot\,;\boldsymbol{\alpha}),\sigma^{(j)},\varepsilon^{(j)}\,\middle|\,t_1^{(j)},\ldots,t_{n^{(j)}}^{(j)},M_1^{(j)},\ldots,M_{n^{(j)}}^{(j)}\right). \tag{16}$$

2.4 Bayesian estimation of model parameters

Our problem is to find a set of unknown parameters $\boldsymbol{\alpha}$, $\boldsymbol{\sigma}$ and $\boldsymbol{\varepsilon}$ that maximize the likelihood in eq. (16) for a given data set $\mathbf{t}$ and $\mathbf{M}$. However, this problem is generally ill-posed, and so we need to use a Bayesian method based on the entropy maximization principle (Akaike 1977, 1980) for unbiased estimation of the unknown parameters. In the present case, we impose roughness penalty (or smoothness constraint) on the slip-rate distribution as prior information, which is defined by the integral of the sum of squares of first- and/or second-order partial derivatives of $\psi(x,y,t;\boldsymbol{\alpha})$ in eq. (14) over the space–time domain (Ogata *et al.* 1991; Yabuki & Matsu'ura 1992). Then, the prior information can be written in a form of PDF as

$$\pi(\boldsymbol{\alpha};\boldsymbol{\omega})=(2\pi)^{-(\dim\boldsymbol{\alpha})/2}[\det\Sigma(\boldsymbol{\omega})]^{1/2}\exp[-\boldsymbol{\alpha}\Sigma(\boldsymbol{\omega})\boldsymbol{\alpha}^{\mathrm{T}}/2], \tag{17}$$

where $\boldsymbol{\omega}$ denotes nonnegative parameters controlling the strength of roughness penalty (or smoothness constraint), and $\Sigma(\boldsymbol{\omega})$ is a positive definite symmetric matrix. In a similar way, we constrain the other parameters $\boldsymbol{\sigma}$ and $\boldsymbol{\varepsilon}$ by introducing their prior probability densities $\pi(\boldsymbol{\sigma};\boldsymbol{\theta})$ and $\pi(\boldsymbol{\varepsilon};\boldsymbol{\xi})$. Both prior distributions prevent the parameters from taking extreme values that may lead to overfitting.

Combining these prior distributions, $\pi(\boldsymbol{\alpha};\boldsymbol{\omega})$, $\pi(\boldsymbol{\sigma};\boldsymbol{\theta})$ and $\pi(\boldsymbol{\varepsilon};\boldsymbol{\xi})$, with the information from observed data in eq. (16), we obtain the likelihood of a Bayesian model:

$$L(\boldsymbol{\alpha},\boldsymbol{\sigma},\boldsymbol{\varepsilon},\boldsymbol{\omega},\boldsymbol{\theta},\boldsymbol{\xi}\,|\,\mathbf{t},\mathbf{M})$$
$$=L_{[t_s,t_e]}(\boldsymbol{\alpha},\boldsymbol{\sigma},\boldsymbol{\varepsilon}\,|\,\mathbf{t},\mathbf{M})\pi(\boldsymbol{\alpha};\boldsymbol{\omega})\pi(\boldsymbol{\sigma};\boldsymbol{\theta})\pi(\boldsymbol{\varepsilon};\boldsymbol{\xi}). \tag{18}$$

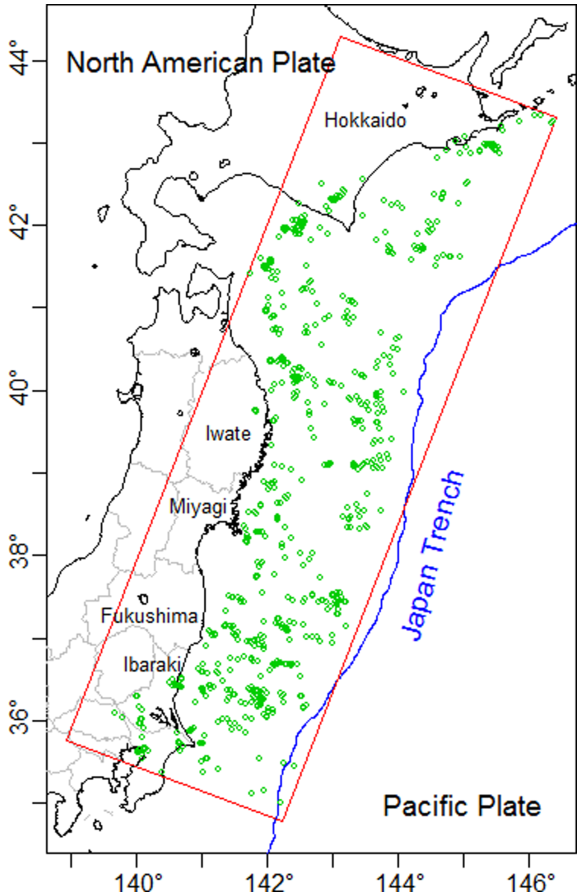

Figure 1. Distribution of repeating earthquakes for 1993–2011. Each green circle indicates the average location of repeating earthquakes in one sequence. The red-boxed area represents the space domain set for the present analysis.

In order to select optimum values of the parameters $(\boldsymbol{\omega}, \boldsymbol{\theta}, \boldsymbol{\xi})$, we maximize the marginal likelihood defined by

$$L(\boldsymbol{\omega}, \boldsymbol{\theta}, \boldsymbol{\xi} \,|\, \mathbf{t}, \mathbf{M}) = \iiint L(\boldsymbol{\alpha}, \boldsymbol{\sigma}, \boldsymbol{\varepsilon}, \boldsymbol{\omega}, \boldsymbol{\theta}, \boldsymbol{\xi} \,|\, \mathbf{t}, \mathbf{M})\, d\boldsymbol{\alpha}\, d\boldsymbol{\sigma}\, d\boldsymbol{\varepsilon}. \quad (19)$$

If we have some choice in parametrization such as the B-spline knots allocation, we can use Akaike's Bayesian Information Criterion (ABIC; Akaike 1980),

$$\mathrm{ABIC} = -2 \max_{\omega,\theta,\xi} \log L(\boldsymbol{\omega}, \boldsymbol{\theta}, \boldsymbol{\xi} \,|\, \mathbf{t}, \mathbf{M}) + 2N, \quad (20)$$

where N is the number of adjustable parameters $(\boldsymbol{\omega}, \boldsymbol{\theta}, \boldsymbol{\xi})$. Given the optimum knots allocation and values of $(\boldsymbol{\omega}, \boldsymbol{\theta}, \boldsymbol{\xi})$, which minimizes ABIC in eq. (20), we can obtain the optimum values of $(\boldsymbol{\alpha}, \boldsymbol{\sigma}, \boldsymbol{\varepsilon})$ by simply maximizing the likelihood in eq. (18).

3 DATA AND MODEL SETTING

We apply the Bayesian statistical method mentioned in the previous section to the complete data set (location, time and magnitude) of repeating earthquakes in northeast Japan for the period from 1993 July 15 to 2011 March 10 (just before the occurrence of the 2011 Tohoku-oki earthquake), reported by Uchida & Matsuzawa (2011, 2013). Sequences of repeating earthquakes are identified through precise analyses of waveform data, recorded by the microearthquake observation network of the Hokkaido University, Hirosaki University, Tohoku University and University of Tokyo. Most of the seismometers are of 1 Hz velocity type and sampling frequency is 100 Hz. The coherency threshold to identify repeating earthquake pairs is common to all the networks. Considering the completeness of event detection off northeast Japan, we selected the sequences whose average magnitudes range from 2.8 to 6.0. Our concern in this study is background slip rates at the North American-Pacific plate interface in northeast Japan, and so we omitted repeating earthquakes at the North American- Philippine Sea plate interface in the Kanto region. The sequences of repeating earthquakes (778 sequences with 2901 events) used for the present analysis are shown in Fig. 1, where each green circle indicates the average location of repeating earthquakes in one sequence.

In order to estimate the space–time distribution of background slip rates from the data set of repeating earthquakes mentioned above, first, we set a space domain as indicated by the red rectangle in Fig. 1, and divided it into 6 × 20 subsections by equally spaced (about 50 km) knots. Then, we divided the time domain (1993 July 15 to 2011 March 10) into 51 subsections by equally spaced (about 4 months) knots for the regions where no large earthquakes ($M > 6.0$) occurred. Within this period, 13 large earthquakes occurred and caused abrupt slip rate changes in 10 different regions on the plate interface (Table 1). Some of them are not so large ($6.0 < M < 6.5$) but triggered many repeating earthquakes as their aftershocks. For these regions, we divided the whole time domain into two parts, pre- and post-seismic periods of the corresponding large earthquake, and allocated unequally spaced (3, 10, 30, and 60 days) knots to properly treat co-seismic abrupt and post-seismic rapid changes in slip rates. Finally, we assigned tri-cubic B-splines to these knots to represent space–time distribution of background slip rates.

Table 1. List of 13 large earthquakes at 10 different regions where the time domain of spline fitting is divided.

Event	Date	Latitude	Longitude	Magnitude	Region and Comment
1-1	1994/12/28	40°25′N	143°44′E	7.6	Far-off-Sanriku
1-2	1995/01/07	40°13′N	142°18′E	7.2	Largest aftershock of Event 1-1
2	1998/05/31	39°01′N	143°50′E	6.4	Off-Sanriku earthquake, triggered 8 repeating events
3-1	2003/09/26	41°46′N	144°04′E	8.0	Tokachi-oki earthquake
3-2	2003/09/26	41°42′N	143°41′E	7.1	Largest aftershock of Event 3-1
4	2003/10/31	37°49′N	142°41′E	6.8	Miyagi-oki
5	2004/11/29	42°56′N	145°16′E	7.1	Kushiro-oki earthquake
6	2008/05/08	36°13′N	141°36′E	7.0	Ibaraki-oki earthquake
7	2008/07/19	37°31′N	142°15′E	6.9	Fukushima-oki earthquake
8	2008/09/11	41°46′N	144°09′E	7.2	Tokachi-oki
9	2010/08/10	39°20′N	143°29′E	6.3	Off-Sanriku earthquake, triggered 8 repeating events
10-1	2011/03/09	38°19′N	143°16′E	7.3	Largest foreshock of Event 10-2
10-2	2011/03/11	38°06′N	142°51′E	9.0	Tohoku-oki earthquake

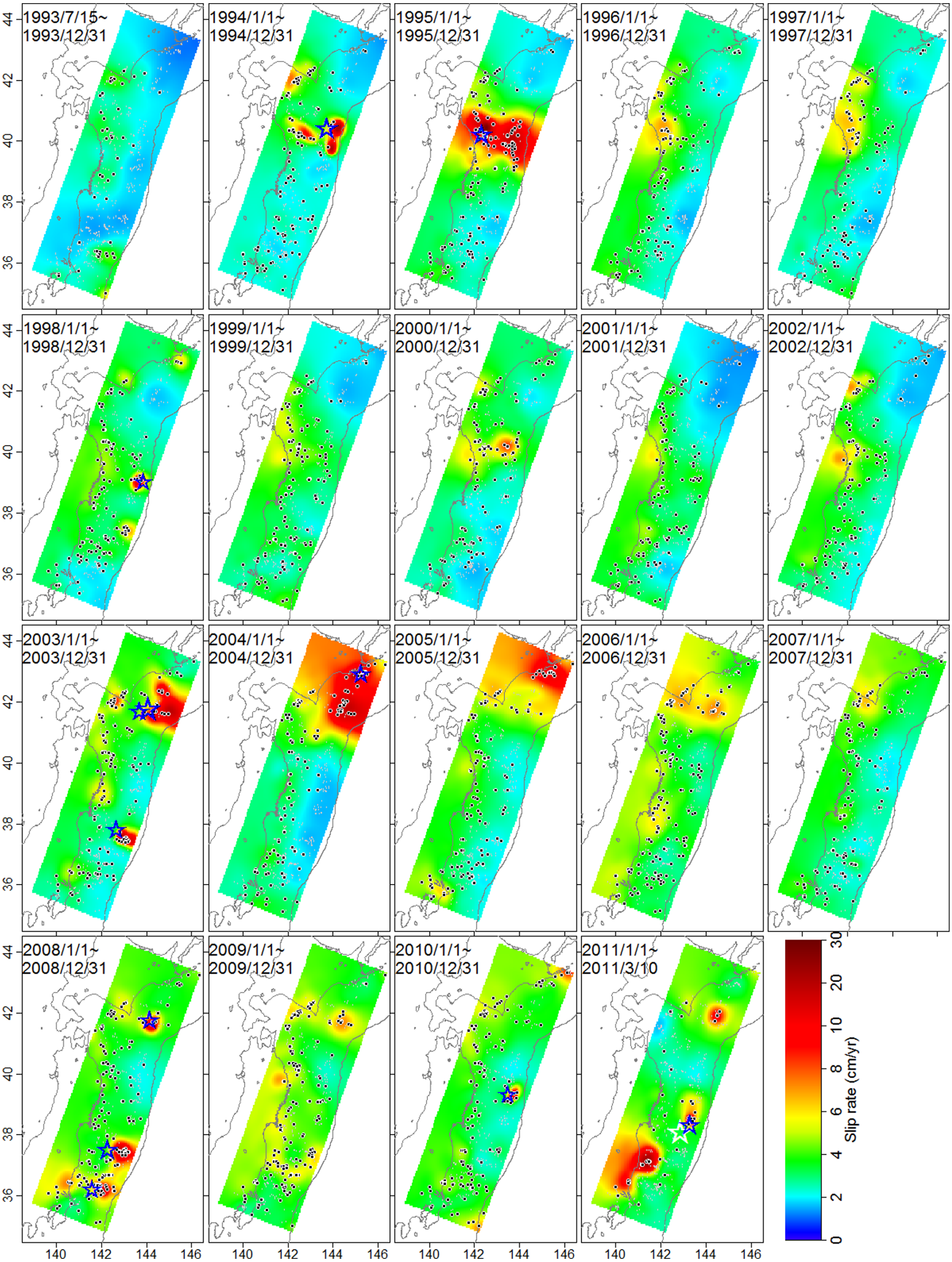

Figure 2. Space–time distribution of interplate slip rates off the Hokkaido-Tohoku region. Each diagram shows the average slip rates (indicated by colour scale) for 1 yr except the first and last periods. The black circles and blue stars represent, respectively, the repeating earthquakes ($2.8 < M < 6.0$) and large interplate earthquakes (listed in Table 1) occurred in the corresponding periods. The white star in the last diagram indicates the epicentre of the 2011 Tohoku-oki earthquake.

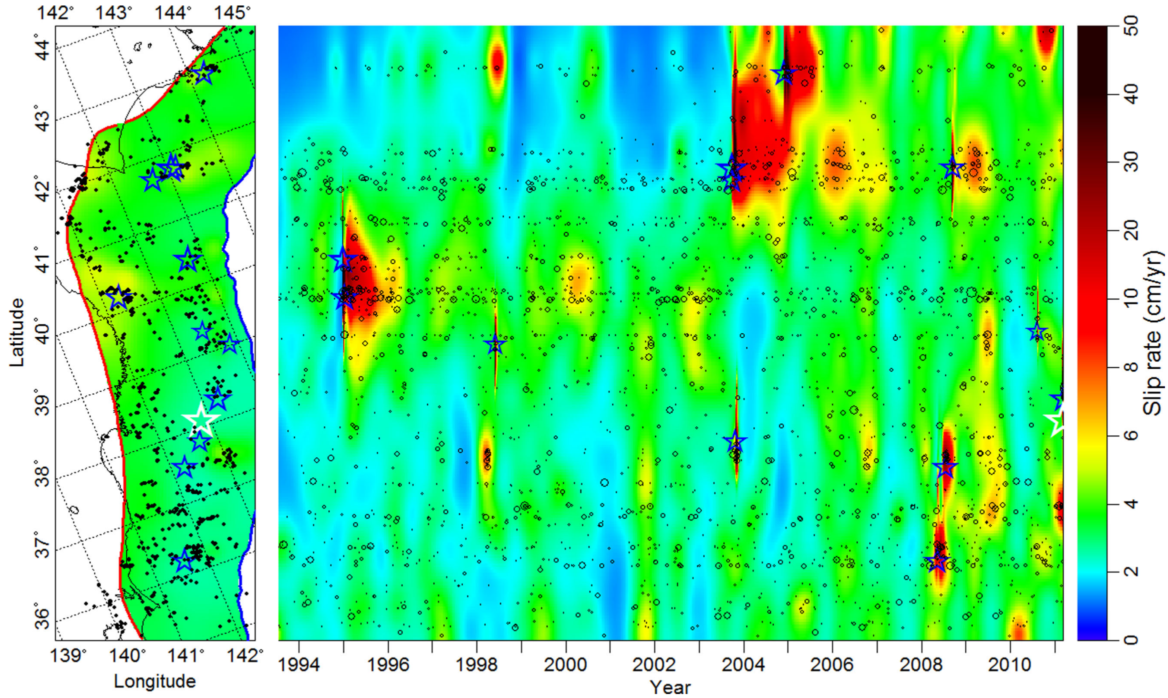

Figure 3. A space–time diagram showing the temporal variation of sip rates associated with large interplate earthquakes. The spatial average of slip rates is taken in a direction nearly parallel to plate convergence. The black circles and blue stars represent, respectively, the repeating earthquakes and large interplate earthquakes (listed in Table 1). The white star indicates the 2011 Tohoku-oki earthquake. For reference, the spatial distribution of the average slip rates over the whole time period is also shown on the left-hand side.

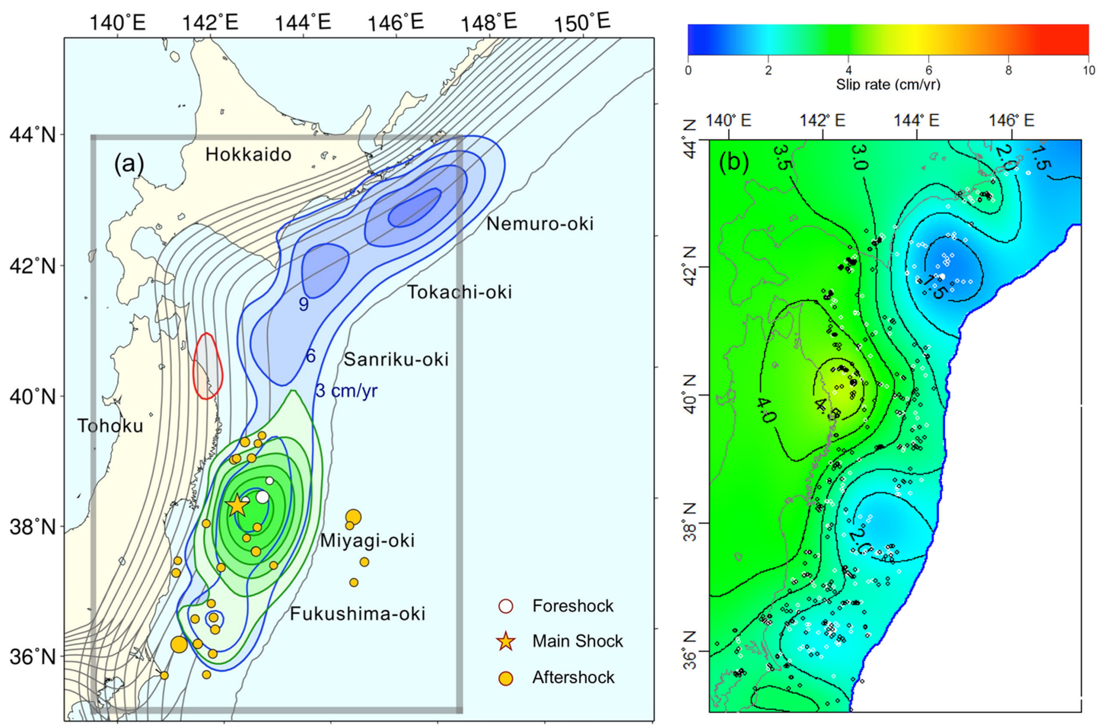

Figure 4. Comparison of interplate slip-rate and slip-deficit-rate distributions in northeast Japan. (a) Average slip-deficit-rate distribution for 1996–2000 estimated from GPS data (after Hashimoto *et al*. 2012). The blue and red contours represent, respectively, slip-deficit and -excess rates at intervals of 3 cm yr^{-1}. For reference, the co-seismic slip distribution of the 2011 Tohoku-oki earthquake is also shown by the green contours at intervals of 4 m. The yellow star indicates the main shock, and the white and yellow circles indicate the foreshocks and aftershocks, respectively. The depth to the upper boundary of the descending Pacific plate, measured from the surface of solid earth, is represented by the grey contours at intervals of 10 km (Hashimoto *et al*. 2004). (b) Average slip-rate distribution for 1996–2000 estimated from repeating earthquake data. The area of this diagram corresponds to the grey-boxed area in (a). The colour scale on the top shows slip rates. The black and white circles represent the repeating earthquakes occurred within and outside the period of 1996–2000, respectively.

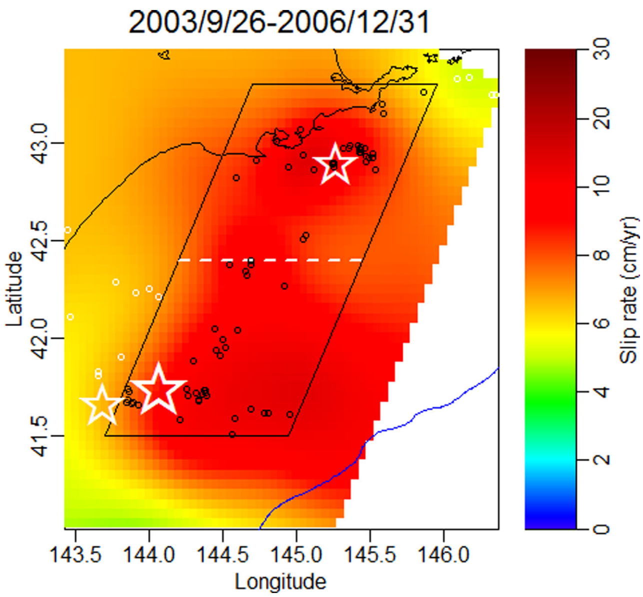

Figure 5. Spatial distribution of the average slip rates for September 2003–December 2006 in the afterslip zone of the 2003 Tokachi-oki earthquake. The white stars represent the large interplate earthquakes occurred in this period.

4 RESULTS OF INVERSION ANALYSIS

We inverted the complete data set of repeating earthquakes in northeast Japan. A series of diagrams in Fig. 2 show the estimated space–time distribution of interplate slip rates off the Hokkaido-Tohoku region for about 18 yr before the 2011 Tohoku-oki earthquake. Here, it should be noted that each diagram represents the average slip rates for the corresponding period (one year except the first and last periods). From this figure, we can see that the background slip rates significantly vary both in space and time. Especially, the occurrence of large earthquakes strongly affects the background slip rates in and around their source regions. For example, the remarkably high slip-rate areas, indicated by red colour, correspond to the 1994 Far-off-Sanriku (M7.6), 2003 Tokachi-oki (M8.0), 2004 Kushiro-oki (M7.1) and 2008 Ibaraki-oki (M7.0) earthquakes.

To see the temporal variation of slip rates associated with the occurrence of large interplate earthquakes, we take the spatial average of slip rates in a direction nearly parallel to plate convergence, and show it as a space–time diagram on the right-hand side of Fig. 3. The diagram on the left-hand side shows the spatial distribution of the average slip rates over the whole time period. From the space–time diagram, we can see that the slip rates abruptly increase just after the occurrence of large earthquakes, which are indicated by blue stars, and gradually decrease with time, reflecting the subsequent afterslip motion. The spatial extent and duration of the postseismic high slip rates are generally wider and longer for larger earthquakes. In addition to these abrupt slip accelerations, there

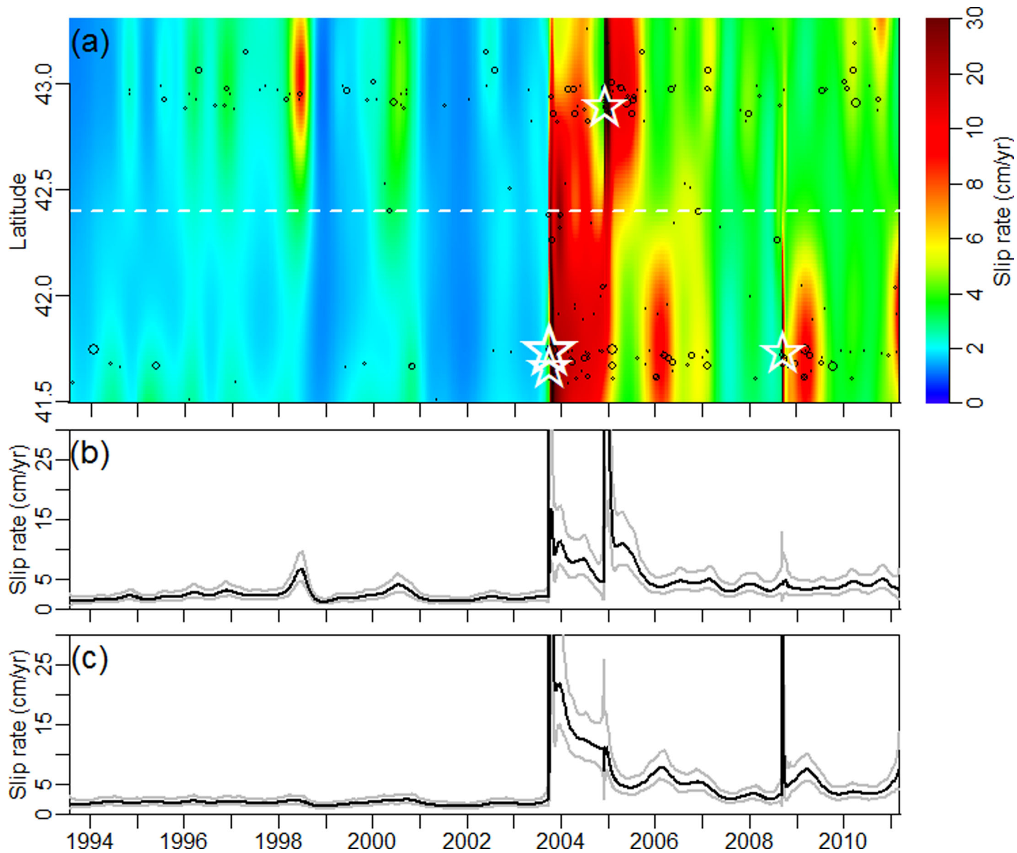

Figure 6. Temporal variation of slip rates associated with the 2003 Tokachi-oki earthquake. (a) A space (latitude)–time diagram showing the slip-rate history in the region southeast off Hokkaido. The upper and lower halves correspond to the Kushiro-oki and Tokachi-oki afterslip zones, respectively, which are indicated in Fig. 5. The black circles and white stars represent, respectively, the repeating earthquakes and large interplate earthquakes occurred in this period. Diagrams (b) and (c) show temporal variation curves of the spatially averaged slip rates in the upper and lower halves in (a), respectively. The grey lines show 95 per cent confidence intervals of the average slip rates.

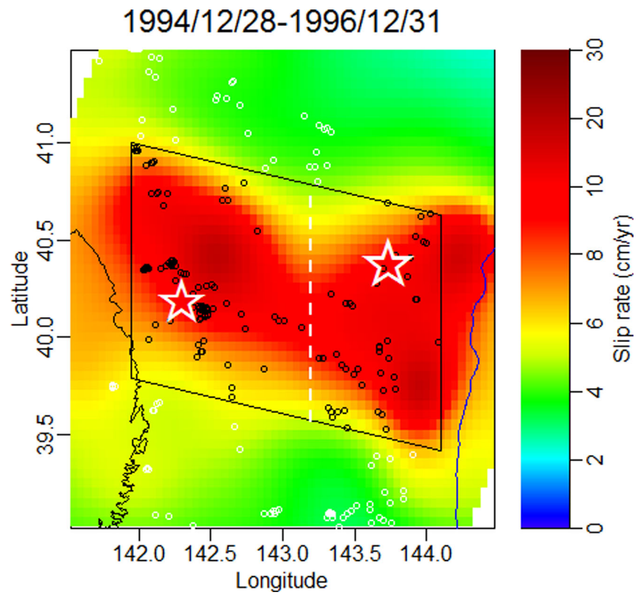

Figure 7. Spatial distribution of the average slip rates for December 1994–December 1996 in the afterslip zone of the 1994 Far-off-Sanriku earthquake. The white stars near the Japan trench and the Sanriku coast indicate the main shock and the largest aftershock of the 1994 Far-off-Sanriku earthquake, respectively.

exist many short-term moderate slip accelerations, which accompany swarm-like seismic activities including several M4–5 events. We can also see that the slip rates off the Hokkaido region have been very low through the period before the occurrence of the 2003 Tokachi-oki earthquake.

In the following part of this section, first, we compare the spatial pattern of average slip rates for a seismically calm period with that of average slip-deficit rates, which has been estimated from GPS array data independently. Then, we examine the temporal variations of slip rates associated with large earthquakes (the 1994 Sanriku-oki, 2003 Tokachi-oki, 2004 Kushiro-oki and 2008 Ibaraki-oki earthquakes) in detail.

4.1 Comparison with the spatial pattern of interseismic slip-deficit rates

For northeast Japan, Hashimoto *et al*. (2009, 2012) have estimated average interplate slip-deficit rates for a seismically calm period (June 1996–May 2000) through the inversion analysis of GPS velocity data (Sagiya 2004). Here, we show the interseismic slip-deficit rate distribution (blue contours) obtained by Hashimoto *et al*. (2012) in Fig. 4(a) together with the co-seismic slip distribution (green contours) of the 2011 Tohoku-oki earthquake. From this figure, we can see that three high slip-deficit rate zones (off Nemuro, Tokachi, and Miyagi) and two moderately high slip-deficit rate zones (off Sanriku and Fukushima) are distributed along the Southern Kuril-Japan trench. These slip-deficit zones are considered to be large-scale

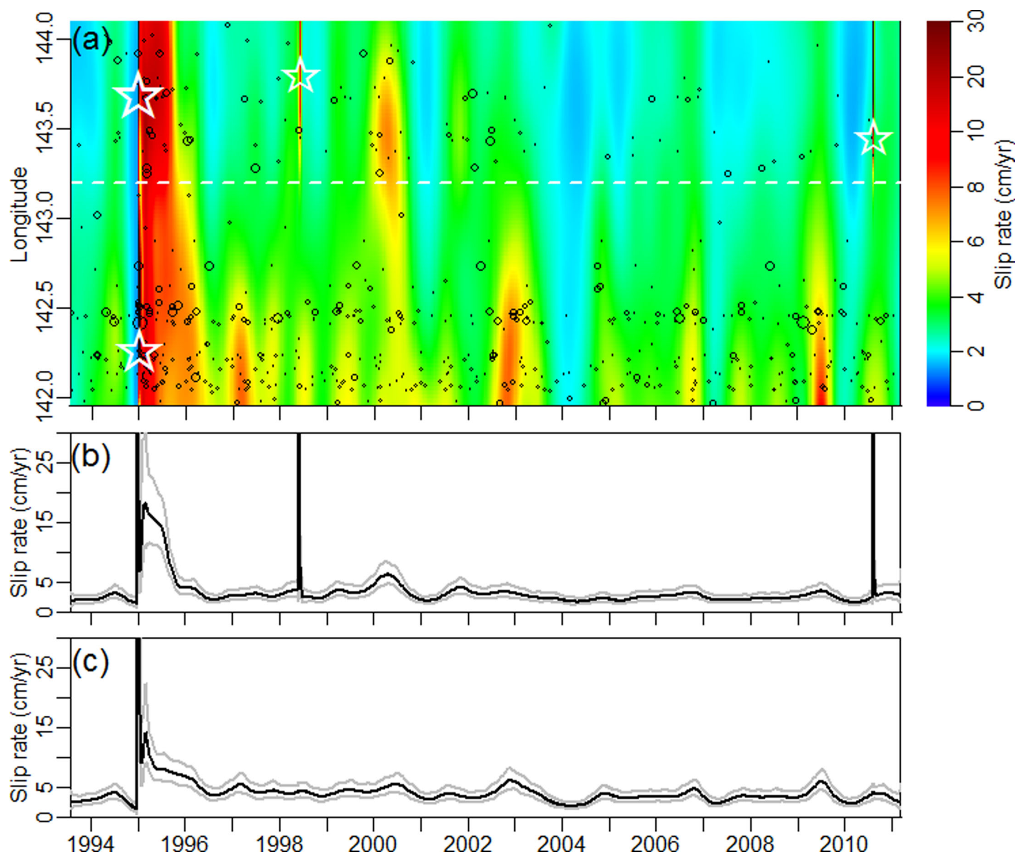

Figure 8. Temporal variation of slip rates off Sanriku. (a) A space (longitude)–time diagram showing the slip-rate history in the shallow main shock region (upper half) and the downdip largest aftershock region (lower half), which are indicated in Fig. 7. The white stars indicate the main shock and the largest aftershock of the 1994 Far-off-Sanriku earthquake, respectively. Diagrams (b) and (c) show temporal variation curves of the spatially averaged slip rates in the upper and lower halves in (a), respectively. The grey lines show 95 per cent confidence intervals of the average slip rates.

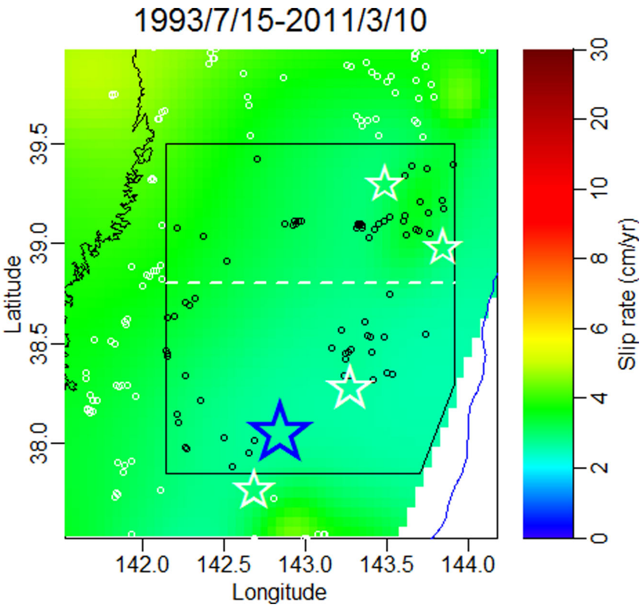

Figure 9. Spatial distribution of the average slip rates for July 1993–March 2011 off Iwate and Miyagi. The large blue star indicates the epicentre of the 2011 Tohoku-oki earthquake. The white stars represent the large interplate earthquakes occurred in this period.

basement asperities, where steady increase of seismogenic stress has continued for the occurrence of forthcoming large earthquakes. Actually, in the Tokachi-oki slip-deficit zone, the M8.0 Tokachi-oki earthquake occurred in 2003, and in the Miyagi-oki and Fukushima-oki slip-deficit zones, the M9.0 Tohoku-oki earthquake occurred in 2011.

It will be interesting to compare the slip-rate distribution estimated from repeating earthquake data with the slip-deficit-rate distribution estimated from GPS array data, because they are expected to be in reciprocal relation. For this purpose, we took the time average of the estimated slip-rate distribution for the same period as in the case of GPS data analysis. The obtained average slip-rate distribution (black contours) in Fig. 4(b) has three low slip-rate zones off Nemuro, Tokachi, and Miyagi, one moderately low slip-rate zone off Fukushima, and one high slip-rate zone near the Sanriku coast. From comparison of Figs 4(a) and (b), we can find a good reciprocal correlation between the average slip rates and the average slip-deficit rates except the region southeast off Nemuro, which is just outside of the coverage of GPS observation network (GEONET). This result indicates the validity of the present statistical method to invert the repeating earthquake data.

4.2 Slip-rate variation southeast off Hokkaido

In the region southeast off Hokkaido, the M8.0 Tokachi-oki and M7.1 Kushiro-oki earthquakes occurred on 2003 September 26 and

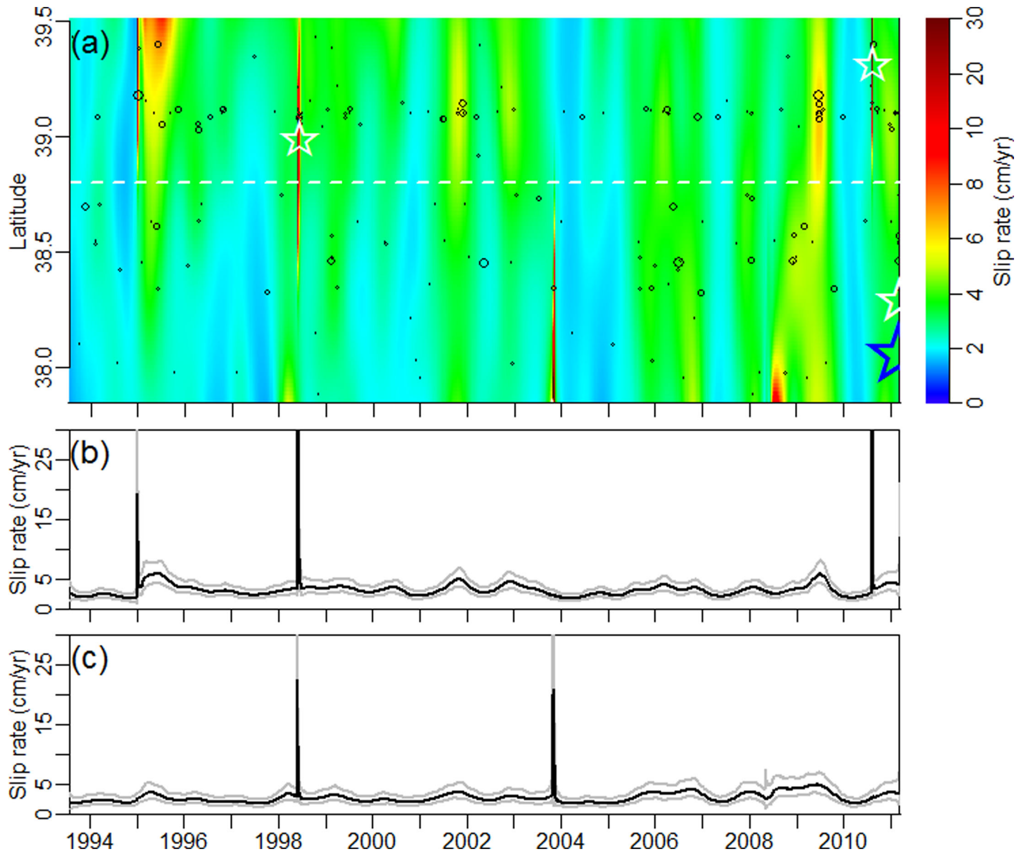

Figure 10. Temporal variation of slip rates off Iwate and Miyagi. (a) A space (latitude)–time diagram showing the slip-rate history in the regions off Iwate (upper half) and Miyagi (lower half), which are indicated in Fig. 9. The large blue star indicates the epicentre of the 2011 Tohoku-oki earthquake. The black circles and white stars represent, respectively, the repeating earthquakes and large interplate earthquakes occurred in this period. Diagrams (b) and (c) show temporal variation curves of the spatially averaged slip rates in the upper and lower halves in (a), respectively. The grey lines show 95 per cent confidence intervals of the average slip rates.

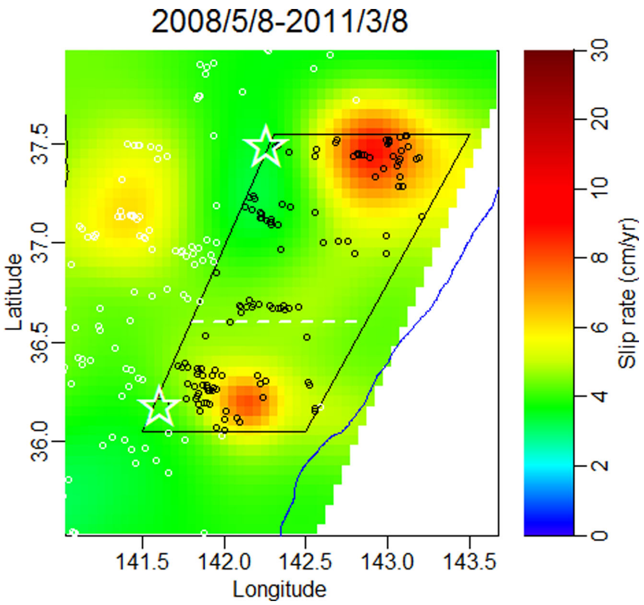

Figure 11. Spatial distribution of the average slip rates for May 2008–March 2011 off Fukushima and Ibaraki. The white stars indicate the epicentres of the 2008 Ibraraki-oki and Fukusima-oki earthquakes.

2004 November 29, respectively. We show the spatial distribution of the average slip rates for September 2003–December 2006 in Fig. 5 and the temporal variation of slip rates associated with these events in Fig. 6 with three diagrams; a space (latitude)–time diagram showing the slip-rate history in the Kushiro-oki (upper half) and Tokachi-oki (lower half) regions (a) and temporal variation curves of the spatially averaged slip rates for the Kushiro-oki and Tokachi-oki regions (b and c).

From Fig. 6(a), we can see that the slip rates have been very low (1–2 cm yr^{-1}) until the 2003 Tokachi-oki earthquake, which is consistent with very high slip-deficit rates there (Fig. 4(a)). The slip rates abruptly increased just after this event, and then gradually decreased with time, reflecting the subsequent afterslip motion. The post-seismic high slip-rate zone propagated toward the northeast and accelerated the occurrence of the 2004 Kushiro-oki earthquake, as pointed out by Ozawa *et al*. (2004) and Murakami *et al*. (2006) from the analysis of GPS data and Uchida *et al*. (2009) from the analysis of both repeating earthquake data and GPS data. In addition, the temporal variation curve of average slip rate in Fig. 6(c) reveals an interesting fact; the slip-rate fluctuation associated with the 2003 Tokachi-oki earthquake has not completely decayed within the observation period. The 95 per cent confidence lower bounds of the average slip rate after the 2003 Tokachi-oki earthquake have kept higher than the average slip rate (2 cm yr^{-1}) before 2003. Since the duration time of afterslip is 1–2 yr at most for interplate earthquakes as seen from Fig. 3, this suggests that 100 km-scale asperities might have a strength-recovery (healing) time longer than 10 yr.

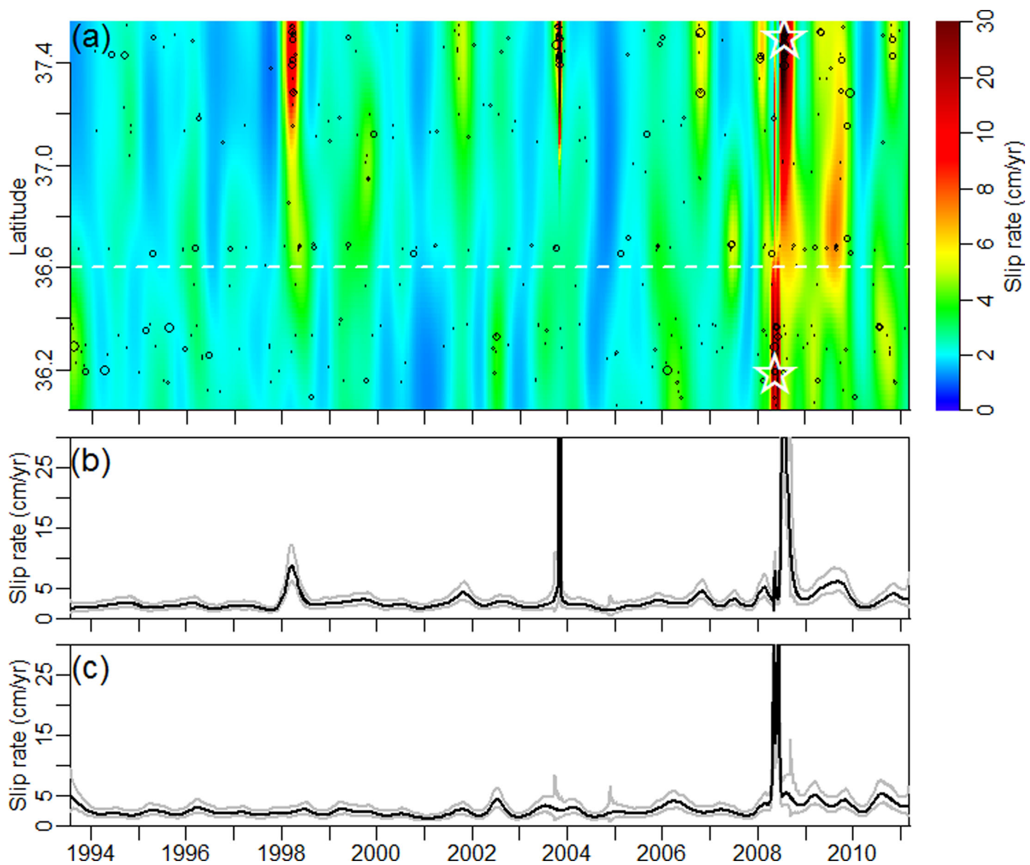

Figure 12. Temporal variation of slip rates off Fukushima and Ibaraki. (a) A space (latitude)–time diagram showing the slip-rate history in the regions off Fukushima (upper half) and Ibaraki (lower half), which are indicated in Fig. 11. The white stars indicate the epicentres of the 2008 Ibraraki-oki and Fukusima-oki earthquakes. Diagrams (b) and (c) show temporal variation curves of the spatially averaged slip rates in the upper and lower halves in (a), respectively. The grey lines show 95 per cent confidence intervals of the average slip rates.

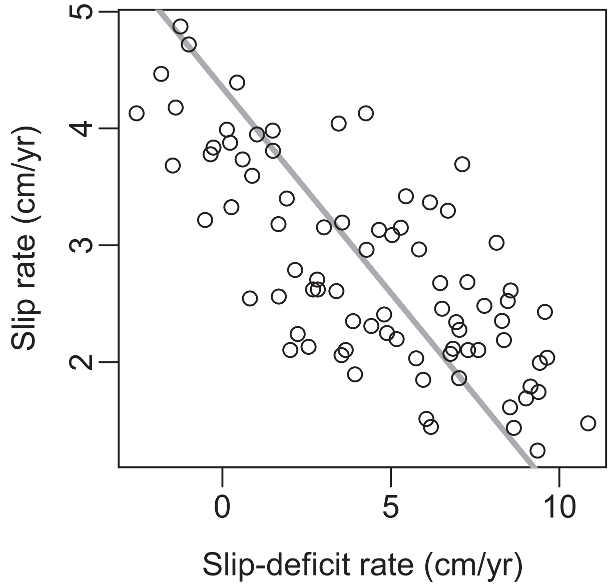

Figure 13. Correlation diagram of the slip rates estimated from repeating earthquake data with the slip-deficit rates estimated from GPS data. The local averages of the slip rates in Fig. 4(b) are plotted against the local average of the slip-deficit rates in Fig. 4(a) at equally spaced (about 50 km) grid points on the plate interface shallower than 80 km. The grey straight line (slope = −0.35, intercept = 4.4) indicates a least-squares fit to the data.

4.3 Slip-rate variation off Sanriku

In the region off Sanriku, the Far-off-Sanriku earthquake (M7.6) occurred on 1994 December 28 and triggered a downdip (near the Sanriku coast) large event (M7.2) on 1995 January 7. In Figs 7 and 8, we show the spatial and temporal variations of slip rates associated with these events in the same way as in Figs 5 and 6. Fig. 7 shows spatial distribution of the average slip rates for December 1994 (just before the main shock)-December 1996, where the white stars near the Japan trench and the Sanriku coast indicate the epicentres of the main shock and its largest aftershock, respectively. Fig. 8(a) is a space (longitude)-time diagram showing the slip-rate history in the shallow main shock region (upper half) and the downdip largest aftershock region (lower half). In Figs 8(b) and (c), we show the temporal variation of the spatially averaged slip rates (black lines) for the main shock and largest aftershock regions, respectively, together with their 95 per cent confidence intervals (grey lines).

From these figures, we can see the significantly low afterslip rate and significantly long afterslip duration for the downdip largest aftershock in comparison with the shallow main shock, which possibly reflects difference in frictional properties with depth. In addition, we can find quasi-periodic moderate slip acceleration at the depths of the seismogenic zone (the lower half of Fig. 8(a)), which corresponds to the quasi-periodic slow-slip behaviour off Sanriku reported by Uchida *et al*. (2016).

4.4 Slip-rate variations preceding the 2011 Tohoku-oki earthquake

The M9.0 Tohoku-oki earthquake occurred on 2011 March 11 so as to release the tectonic stress accumulated in the Miyagi-oki and Fukushima-oki interseismic slip-deficit zones (e.g. Loveless & Meade 2011; Hashimoto *et al*. 2012). Kato *et al*. (2012) revealed that the dynamic rupture of this earthquake was preceded by the migrating foreshock sequence broken out just after the M7.3 event on 2011 March 9. In addition to such a short-term precursor, Mavrommatis *et al*. (2014, 2015) have reported long-term acceleration of aseismic slip preceding the Tohoku-oki earthquake from the analysis of GPS data and repeating earthquake data both in the period from 1996 to 2011.

We show the spatial and temporal variations of aseismic slip rates preceding the Tohoku-oki earthquake in Figs 9 and 10 for the region off Iwate and Miyagi and Figs 11 and 12 for the region off Fukushima and Ibaraki in the same way as in Figs 5 and 6. Fig. 9 shows the average slip rates off Iwate and Miyagi for July 1993–March 2011, where the large blue star indicates the epicentre of the 2011 Tohoku-oki earthquake. On the other hand, Fig. 11 shows the average slip rates off Fukushima and Ibaraki for May 2008–March 2011, where the white stars indicate the epicentres of the 2008 Ibraraki-oki (M7.0) and Fukushima-oki (M6.9) earthquakes.

Fig. 10(a) is a space (latitude)-time diagram showing the slip-rate history off Iwate (upper half) and off Miyagi (lower half). From the slip-rate history off Miyagi, we can see that the main rupture zone of the Tohoku-oki earthquake has been in a low slip-rate state until the occurrence of the M9.0 event, which is consistent with high slip-deficit rates there (Fig. 4a). The pre-seismic low slip rate in the main rupture zone is more clearly shown by the temporal variation curve of spatially averaged slip rates in Fig. 10(c). Fig. 12(a) is a space (latitude)-time diagram showing the slip-rate history off Fukushima (upper half) and off Ibaraki (lower half). From the slip-rate history in these regions, where an M8-class secondary rupture was dynamically triggered by the main rupture in 2011, we can see that a low slip-rate state has continued until the occurrence of two M7-class events in 2008, except some moderate slip-rate increases occurred off Fukushima. From the temporal variation curves of spatially averaged slip rates in Figs 12(b) and (c), we can see that the slip rates abruptly increased just after these events, and then rapidly decreased to a slightly higher level (3–5 cm yr^{-1}) than before (2–3 cm yr^{-1}). As pointed out by Suito *et al*. (2011), the afterslip of the M6.9 Fukushima-oki earthquake has an unusually large amplitude and extent, but its duration time is not unusual. From the present analysis, we could not find long-term (decadal-scale) acceleration of aseismic slip preceding the Tohoku-oki earthquake.

5 DISCUSSION

In Section 4.1, we compared the average slip-rate distribution estimated from repeating earthquake data with the average slip-deficit-rate distribution estimated from GPS array data for a seismically calm period (1996–2000), and found good reciprocal correlation between their spatial patterns except the region southeast off Nemuro, which is just outside of the coverage of GPS observation network. In Fig. 13, to confirm this reciprocal correlation, we plotted the local averages of the slip rates in Fig. 4(b) against the local averages of the slip-deficit rates in Fig. 4(a) at equally spaced (about 50 km) grid points on the plate interface shallower than 80 km. Here, the local average is taken over the about 50 km-squared area with its centre at a grid point both in slip rates and slip-deficit rates. From this diagram, we obtain the negative correlation coefficient of −0.74. The grey straight line (slope = −0.35, intercept = 4.4) indicates a least-squares fit to the data.

What we can estimate from repeating earthquake data is the background slip rates for small asperities. On the other hand, what we can estimate from GPS array data is the slip-deficit rates of underlying large-scale asperities. So, the sum of the slip rate and the slip-deficit rates must be equal to a plate convergence rate

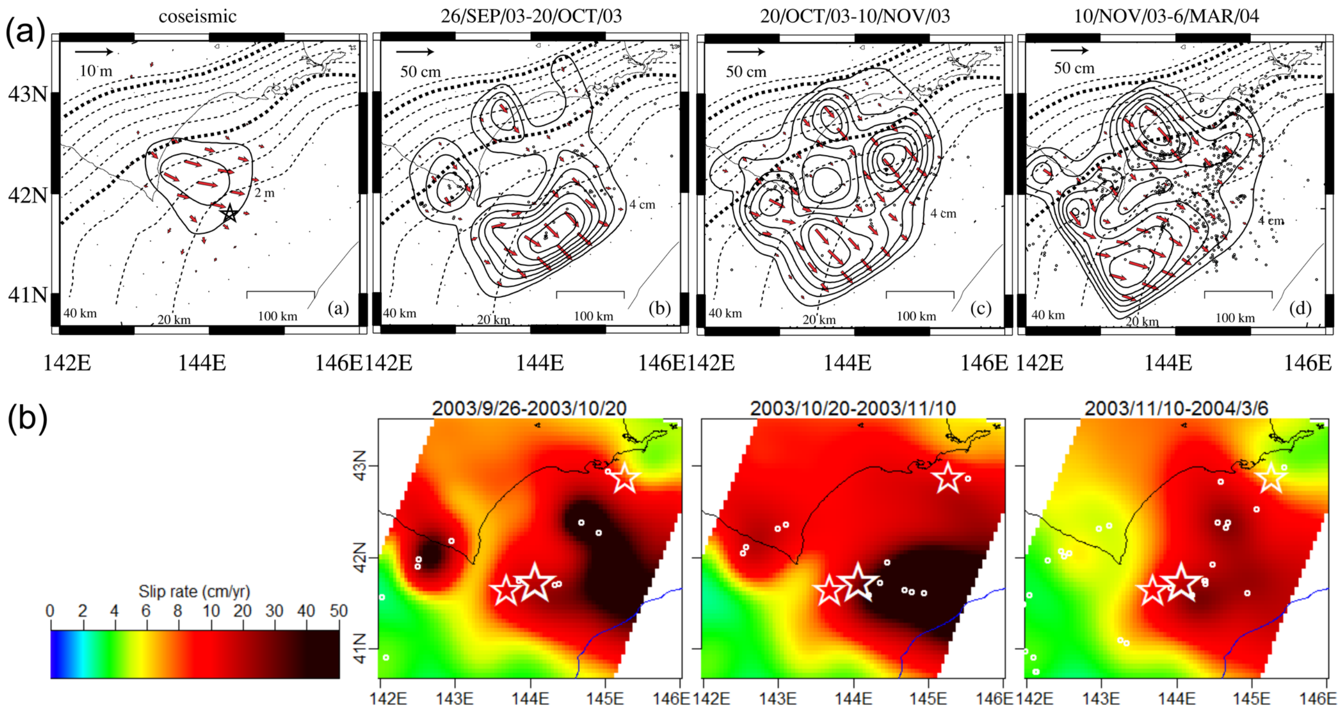

Figure 14. Spatiotemporal changes in post-seismic slip of the 2003 Tokachi-oki earthquake. (a) Co-seismic and post-seismic slip distributions estimated from GPS array data (after Ozawa *et al.* 2004). Contour intervals are 2 m for co-seismic slip and 4 cm for post-seismic slip, respectively. (b) Post-seismic slip rate distributions for the same periods as in (a) estimated from repeating earthquake data. The white circles and stars represent, respectively, the repeating earthquakes and large interplate earthquakes occurred in the whole period (2003 September 26 to 2004 March 6).

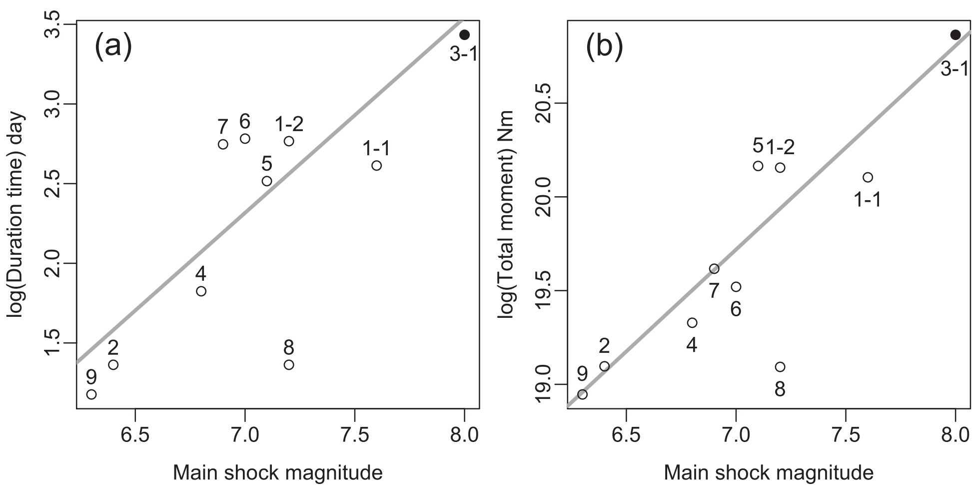

Figure 15. The duration time and total moment of afterslip plotted against the magnitude of main shock for the large interplate earthquakes. The event numbers correspond to those in Table 1. (a) Logarithm of the duration time of afterslip plotted against main shock magnitude. The solid circle means that the decay of slip rate is incomplete within the observation period. (b) Logarithm of the total moment of afterslip plotted against main shock magnitude. In either diagram, the grey straight line indicates a least-squares fit to the data. The slope and intercept of these lines are 1.2 and −6.3 for (a) and 1.1 and 12.1 for (b).

(8–9 cm yr^{-1} in northeast Japan) within some estimation error range. However, even after taking into account the estimation errors of slip-deficit rates (2–4 cm yr^{-1}), the amplitude of estimated slip-rate distribution is a bit small to satisfy the postulation mentioned above. The bias in amplitude may be responsible for the empirical relation between recurrence intervals and magnitudes of repeating earthquakes in eq. (7), which scales the amplitude of slip rates.

In Section 4.2, we examined the spatiotemporal variation of slip rates in the region southeast off Hokkaido, and revealed that the post-seismic high slip-rate zone associated with the 2003 Tokachi-oki earthquake propagated toward the northeast and accelerated the occurrence of the 2004 Kushiro-oki earthquake. From the time-dependent inversion analysis of GPS data, Ozawa *et al.* (2004) have also revealed the temporal variation of post-seismic slip distribution for the 2003 Tokachi-oki earthquake in detail. It will be interesting to compare our results estimated from repeating earthquake data with their results estimated from GPS data. A series of diagrams in Fig. 14(a) show the co-seismic slip distribution and the post-seismic slip distributions for a sequential three periods (2003/9/26–2003/10/20; 2003/10/20–2003/11/10; 2003/11/10–2004/3/6).

Contour intervals are 2 m for co-seismic slip and 4 cm for post-seismic slip, respectively. A series of diagrams in Fig. 14(b) show the post-seismic slip-rate distributions estimated from repeating earthquake data for the same sequential periods as in Fig. 14(a). In both cases, the post-seismic slip region surrounding the co-seismic slip zone gradually extends with time and propagates toward the northeast. Similarity in the evolution pattern of post-seismic slip suggests consistency between the inversion analyses of GPS array data and repeating earthquake data.

In the present analysis, we examined the temporal variation of post-seismic slip rates in detail for 13 large interplate earthquakes, and found a general tendency that the spatial extent and duration of post-seismic high slip rates are wider and longer for larger earthquakes. We can roughly evaluate the duration times and total moments of afterslips from the temporal variation curves and space–time diagrams in Figs 6, 8, 10 and 12. In Figs 15(a) and (b), we plotted the duration time and total moment of afterslip against the magnitude of main shock, respectively, for the 13 large interplate earthquakes listed in Table 1. Here, we defined the duration time of afterslip as the decay time of post-seismic high slip rate in the temporal variation curve. Then, we calculated the total moment of afterslip from the space–time diagram with the average crustal rigidity of 40 GPa. In either case of the duration time and the total moment, we can see some log-linear relationship (the solid straight line indicates a least-squares fit to the data). Among the 13 earthquakes, the event 8 (the 2008 Tokachi-oki earthquake) seems to be exceptional; both the duration time and total moment of its afterslip are abnormally short and small.

6 CONCLUSIONS

Repeating earthquakes are physically understood as the cyclic process of stress accumulation and release at small asperities distributed on a plate interface. Based on such understanding, we modelled a sequence of repeating earthquakes as a non-stationary renewal process. An advantage of the stochastic modelling is that we can use information of quiescence before the first event and that after the last event of a sequence as well as occurrence times of repeating earthquakes on the theory of point processes.

So far, because of the use of simple least-square methods, the estimation of slip rates has been limited to specific space–time domains where a sufficiently large number of repeating earthquakes occurred. To overcome such situation, we developed a Bayesian statistical method to estimate the space–time distribution of interplate slip rates from the recurrence intervals of repeating earthquakes. In this method, the space–time distribution of slip rates is represented by the superposition of tri-cubic B-splines. The knots of B-splines in time are unequally allocated for representing co-seismic abrupt and post-seismic rapid changes in slip rates. In addition, to avoid overfitting, smoothness constraint is imposed and its optimal weight is determined by ABIC.

We applied the Bayesian statistical method to the complete data set of repeating earthquakes in northeast Japan from 1993 July 15 to 2011 March 10, and estimated space–time distribution of interplate slip rates off Hokkaido and Tohoku for about 18 yr before the 2011 Tohoku-oki earthquake. From the space–time diagram showing slip-rate history, we can see that the slip rates abruptly increase just after the occurrence of large earthquakes, and gradually decrease with time, reflecting the subsequent afterslip motion. The spatial extent and duration of the post-seismic high slip rates are generally wider and longer for larger earthquakes.

To check the validity of the present method, we compared the average slip-rate distribution estimated from repeating earthquake data with the average slip-deficit-rate distribution estimated from GPS array data for a seismically calm period (1996–2000), and confirmed good reciprocal correlation between their spatial patterns. This means that repeating earthquake data and GPS array data provide us with complementary information about interplate aseismic slip rates.

In the region off Hokkaido and Tohoku, the 1994 Sanriku-oki (M7.6), 2003 Tokachi-oki (M8.0), 2004 Kushiro-oki (M7.1) and 2008 Ibaraki-oki (M7.0) earthquakes occurred before the 2011 Tohoku-oki earthquake. We examined the temporal changes of slip rates associated with these earthquakes in detail, and obtained some interesting results as follows. In the region southeast off Hokkaido, the slip rates have been very low until the 2003 Tokachi-oki earthquake. After the co-seismic increase of slip rates, the post-seismic high slip-rate zone propagated toward the northeast and accelerated the occurrence of the 2004 Kushiro-oki earthquake. The slip-rate fluctuation associated with the 2003 Tokachi-oki earthquake has not completely decayed within the observation period, indicating very slow strength-recovery (healing) of large-scale asperities. In the region off Sanriku, the afterslip duration time at the deep seismogenic zone is much longer than that at the shallow seismogenic zone, possibly reflecting difference in frictional properties with depth. At the depths of the seismogenic zone, quasi-periodic moderate slip acceleration is observed.

The main rupture zone of the Tohoku-oki earthquake off Miyagi has been in a low slip-rate state until the occurrence of the M9.0 event. In the region off Fukushima and Ibaraki, where the main rupture triggered an M8-class secondary rupture, a low slip-rate state has continued until the occurrence of two M7-class events in 2008. The slip rates abruptly increased just after these events, and then rapidly decreased to a slightly higher level than before.

ACKNOWLEDGEMENTS

We thank the editor Egill Hauksson and two anonymous reviewers. Thoughtful comments from them were helpful to improve the manuscript. We also thank Chihiro Hashimoto for providing numerical data of interplate slip-deficit rates in northeast Japan and Hokkaido University, Hirosaki University, Tohoku University and University of Tokyo for providing waveform data. This work was supported by JSPS KAKENHI Grant Numbers JP26870193 and JP26240004.

REFERENCES

Akaike, H., 1977. On entropy maximization principle, in *Application of Statistics*, pp. 27–41, ed. Krishnaiah, P.R., North-Holland.

Akaike, H., 1980. Likelihood and Bayes procedure, in *Bayesian Statistics*, pp. 143–166, eds Bernardo, J.M., DeGroot, M.H., Lindley, D.V. & Smith, A.F.M., Valencia University Press.

Daley, D. & Vere-Jones, D., 1988. *An Introduction to the Theory of Point Processes,* Springer-Verlag.

de Boor, C., 1978. *A Practical Guide to Splines,* Springer-Verlag.

Fukuyama, E., Hashimoto, C. & Matsu'ura, M., 2002. Simulation of the transition of earthquake rupture from quasi-static growth to dynamic propagation, *Pure appl. Geophys.,* **159,** 2057–2066.

Hanks, T.C. & Kanamori, H., 1979. A moment magnitude scale, *J. geophys. Res.,* **84,** 2348–2349.

Hashimoto, C. & Matsu'ura, M., 2000. 3-D physical modelling of stress accumulation and release processes at transcurrent plate boundaries, *Pure appl. Geophys.,* **157,** 2125–2147.

Hashimoto, C. & Matsu'ura, M., 2002. 3-D simulation of earthquake generation cycles and evolution of fault constitutive properties, *Pure appl. Geophys.,* **159,** 2175–2199.

Hashimoto, C., Fukui, K. & Matsu'ura, M., 2004. 3-D Modelling of plate interfaces and numerical simulation of long-term crustal deformation in and around Japan, *Pure appl. Geophys.,* **161,** 2053–2067.

Hashimoto, C., Noda, A., Sagiya, T. & Matsu'ura, M., 2009. Interplate seismogenic zones along the Kuril-Japan trench inferred from GPS data inversion, *Nat. Geosci.,* **2,** 141–144.

Hashimoto, C., Noda, A. & Matsu'ura, M., 2012. The M_w 9.0 northeast Japan earthquake: total rupture of a basement asperity, *Geophys. J. Int.,* **189,** 1–5.

Hashimoto, C., Fukuyama, E. & Matsu'ura, M., 2014. Physics-based 3-D simulation for earthquake generation cycles at plate interfaces in subduction zones, *Pure appl. Geophys.,* **171,** 1705–1728.

Igarashi, T., Matsuzawa, T. & Hasegawa, A., 2003. Repeating earthquakes and interplate aseismic slip in the northeastern Japan subduction zone, *J. geophys. Res.,* **108,** 2249, doi:10.1029/2002JB001920.

Kanamori, H., 1977. The energy release in great earthquakes, *J. geophys. Res.,* **82,** 2981–2987.

Kato, A., Obara, K., Igarashi, T., Tsuruoka, H., Nakagawa, S. & Hirata, N., 2012. Propagation of slow slip leading up to the 2011 M_w 9.0 Tohoku-oki earthquake, *Science,* **335,** 705–708.

Lay, T. & Kanamori, H., 1981. An asperity model of great earthquake sequences, in *Earthquake Prediction: An International Review*, pp. 579–592, eds Simpson, W. & Richards, G., Maurice Ewing Ser. 4, AGU.

Lindqvist, B.H., Elvebakk, G. & Heggland, K., 2003. The trend-renewal process for statistical analysis of repairable systems, *Technometrics,* **45,** 31–44.

Loveless, J.P. & Meade, B.J., 2011. Spatial correlation of interseismic coupling and coseismic rupture extent of the 2011 $M_w = 9.0$ Tohoku-oki earthquake, *Geophys. Res. Lett.,* **38,** doi:10.1029/2011GL048561.

Matthews, M.V., Ellsworth, W.L. & Reasenberg, P.A., 2002. A Brownian model for recurrent earthquakes, *Bull. seism. Soc. Am.,* **92,** 2233–2250.

Mavrommatis, A.P., Segall, P. & Johnson, K.M., 2014. A decadal-scale deformation transient prior to the 2011 M_w 9.0 Tohoku-oki earthquake, *Geophys. Res. Lett.,* **41,** doi:10.1002/2014GL060139.

Mavrommatis, A.P., Segall, P., Uchida, N. & Johnson, K.M., 2015. Long-term acceleration of aseismic slip preceding the M_w 9 Tohoku-oki earthquake: constraints from repeating earthquakes, *Geophys. Res. Lett.,* **42,** 9717–9725.

Murakami, M., Suito, H., Ozawa, S. & Kaidzu, M., 2006. Earthquake triggering by migrating slow slip initiated by M8 earthquake along Kuril Trench, Japan, *Geophys. Res. Lett.,* **33,** doi:10.1029/2006GL025967.

Nadeau, R.M. & Johnson, L.R., 1998. Seismological studies at Parkfield VI: moment release rates and estimates of source parameters for small repeating earthquakes, *Bull. seism. Soc. Am.,* **88,** 790–814.

Nadeau, R.M. & McEvilly, T.V., 1999. Fault slip rates at depth from recurrence intervals of repeating microearthquakes, *Science,* **285,** 718–721.

Nadeau, R.M., Foxall, W. & McEvilly, T.V., 1995. Clustering and periodic recurrence of microearthquakes on the San Andreas Fault, California, *Science,* **267,** 503–507.

Nomura, S., Ogata, Y. & Nadeau, R.M., 2014. Space-time model for repeating earthquakes and analysis of recurrence intervals on the San Andreas Fault near Parkfield, California, *J. geophys. Res.,* **119,** 7092–7122.

Ogata, Y., Imoto, M. & Katsura, K., 1991. 3-D spatial variation of b-values of magnitude-frequency distribution beneath the Kanto District, Japan, *Geophys. J. Int.,* **104,** 135–146.

Ozawa, S., Kaidzu, M., Murakami, M., Imakiire, T. & Hatanaka, Y., 2004. Coseismic and postseismic crustal deformation after the M_w 8 Tokachi-Oki earthquake in Japan, *Earth Planets Space,* **56,** 675–680.

Sagiya, T., 2004. Interplate coupling in the Kanto district, central Japan, and the Boso peninsula silent earthquake in May 1996, *Pure appl. Geophys.,* **161,** 2327–2342.

Suito, H., Nishimura, T., Tobita, M., Imakiire, T. & Ozawa, S., 2011. Interplate fault slip along the Japan trench before the occurrence of the 2011 off the Pacific coast of Tohoku earthquake as inferred from GPS data, *Earth Planets Space,* **63,** 615–619.

Uchida, N. & Matsuzawa, T., 2011. Coupling coefficient, hierarchical structure, and earthquake cycle for the source area of the 2011 off the Pacific coast of Tohoku earthquake inferred from small repeating earthquake data, *Earth Planets Space,* **63,** 675–679.

Uchida, N. & Matsuzawa, T., 2013. Pre- and postseismic slow slip surrounding the 2011 Tohoku-oki earthquake rupture, *Earth planet. Sci. Lett.,* **374,** 81–91.

Uchida, N., Hasegawa, A., Matsuzawa, T. & Igarashi, T., 2004. Pre- and post-seismic slow slip on the plate boundary off Sanriku, NE Japan associated with three interplate earthquakes as estimated from small repeating earthquake data, *Tectonophysics,* **385,** 1–15.

Uchida, N., Yui, S., Miura, S., Matsuzawa, T., Hasegawa, A., Motoya, Y. & Kasahara, M., 2009. Quasi-static slip on the plate boundary associated with the 2003 M8.0 Tokachi-oki and 2004 M7.1 off-Kushiro earthquakes, Japan, *Gondwana Res.,* **16,** 527–533.

Uchida, N., Iimura, T., Nadeau, R.M., Bürgmann, R. & Hino, R., 2016. Periodic slow slip triggers megathrust zone earthquakes in northeastern Japan, *Science,* **351,** 488–492.

Yabuki, T. & Matsu'ura, M., 1992. Geodetic data inversion using a Bayesian information criterion for spatial distribution of fault slip, *Geophys. J. Int.,* **109,** 363–375.